UniChromCD for Demultiplexing Time-resolved Charge Detection-Mass Spectrometry Data

Sanders, James D.[1]; Owen, October N.[1]; Tran, Brian H.[1]; Juetten, Kyle J.[2]; Marty, Michael T.[1*]

[1]Department of Chemistry and Biochemistry, University of Arizona, Tucson, Arizona, 85719, United States

[2]Department of Chemistry, The University of Texas at Austin, Austin, Texas, 78712, United States

ABSTRACT: Charge detection mass spectrometry (CD-MS) enables characterization of large, heterogeneous analytes through the analysis of individual ion signals. Because hundreds to thousands of scans must be acquired to produce adequate ion statistics, CD-MS generally requires long analysis times. The slow acquisition speed of CD-MS complicates efforts to couple it with time-dispersive techniques, such as chromatography and ion mobility, because it is not always possible to acquire enough scans from a single sample injection to generate sufficient ion statistics. Multiplexing methods based on Hadamard and Fourier transforms offer an attractive solution to this problem by improving the duty cycle of the separation while preserving retention/drift time information. However, integrating multiplexing with CD-MS data processing is complex. Here, we present UniChromCD, a new module in the open-source UniDec package that incorporates CD-MS time-domain data processing with demultiplexing tools. Following a detailed description of the algorithm, we demonstrate its capabilities using two multiplexed CD-MS workflows: Hadamard-transform size-exclusion chromatography and Fourier-transform ion mobility. Overall, UniChromCD provides a user-friendly interface for analysis and visualization of time-resolved CD-MS data.

INTRODUCTION

Charge detection-mass spectrometry (CD-MS) is uniquely powerful for studying large and/or heterogeneous biomolecules where conventional MS techniques fail due to lack of well-defined charge state distributions or isotopic envelopes typically used to identify charge states.[1–4] In particular, CD-MS has found applications in the analysis of virus capsids,[5,6] lipoproteins,[7] exosomes,[8] nanoparticles,[9] and heavily-modified proteins.[10] By analyzing only a few ions at a time, CD-MS takes advantage of the fact that the magnitude of an ion's induced current signal scales directly with the charge state of the ion, allowing charge states to be assigned for each ion based on a calibration of intensity vs. charge.

Because CD-MS only analyzes a few ions at a time, hundreds or thousands of scans are often needed to produce high-quality data. Thus, coupling CD-MS to time dispersive separation techniques such as liquid chromatography (LC) and ion mobility (IM) presents a challenge due to an inherent duty cycle mismatch. Previous efforts to couple CD-MS with LC[11,12] and capillary electrophoresis (CE)[13] have achieved some success, although spectra had relatively low signal-to-noise ratios (SNR). At the time of writing, we are not aware of any studies that report coupling IM with CD-MS, but information about collision cross sections (CCS) has been obtained through analysis of signal decay rates in ELIT[14,15] and Orbitrap[16] CD-MS platforms.

One strategy for addressing duty cycle mismatch is with multiplexed injections. Multiplexing of gas chromatography (GC),[17,18] LC,[19,20] and CE[21,22] injections using Hadamard transform (HT) has been shown to improve throughput and SNR. Using a variety of injection apparatuses, a sample is injected onto the column multiple times in close succession according to a pseudo-random binary sequence (PRBS). The resulting chromatogram, which contains multiple peaks for each analyte in the sample, is then demultiplexed using an inverse Hadamard transform, yielding a single peak for each analyte with a demultiplexed area equal to the sum of the areas of all corresponding peaks in the multiplexed chromatogram.

Coupling IM with MS can also benefit from multiplexing to improve SNR and resolve the duty cycle mismatch. Both HT[23,24] and Fourier transform (FT)[25–28] multiplexing techniques have been used in these applications, usually in conjunction with the addition of a second ion gate at the end of the mobility cell to modulate ions both entering and exiting the cell. In FT multiplexing, both ion gates are modulated by a square wave frequency sweep to create an oscillating ion signal, the frequency of which corelates with the arrival time of the ions. The chromatogram is demultiplexed by first performing a Fourier transform and then dividing the resulting frequency axis by the sweep rate used to modulate the gates.

Both HT and FT multiplexing strategies offer a substantial improvement in duty cycle, defined here as the fraction of total MS scans that contain useful ion signals, and are thus attractive options to improve the throughput of time-dispersive separation methods with CD-MS. However, the incorporation of CD-MS data into demultiplexing workflows adds significant complexity because each scan must be processed to extract *m/z* and charge information, and the high scan-to-scan variability inherent to CD-MS data often produces noisy and inconsistent features in time-domain data. Here, we describe a free and open-source software package, UniChromCD (UCCD), to process time-resolved CD-MS data, perform both HT and FT demultiplexing operations, and perform many post-processing tasks such as removal of HT spectral artifacts and calculating CCS from demultiplexed IM data.

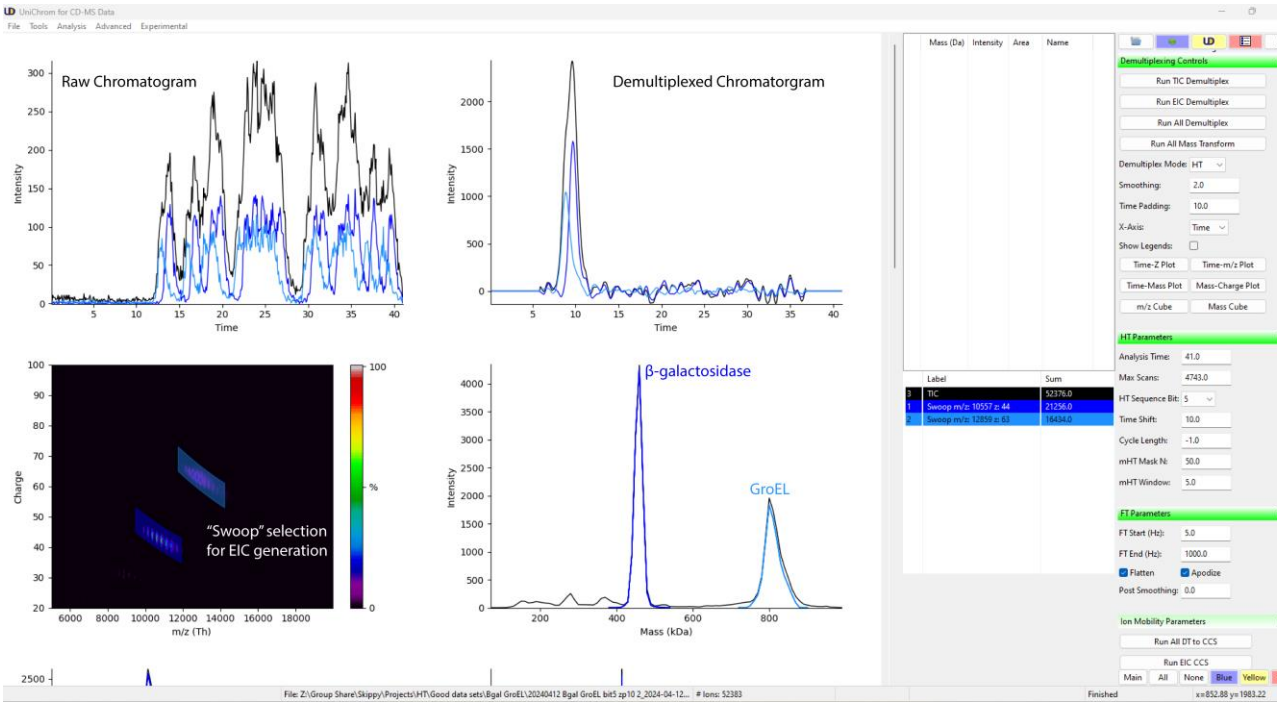

Figure 1. UCCD GUI with example data displayed. The raw chromatogram and EICs are displayed in the top left plot. Demultiplexed chromatograms/arrival time distributions are displayed in the top right plot. A 2D m/z vs. charge histogram of CD-MS data is displayed in the bottom left plot, and the mass distribution in the bottom right. Additional plots are not shown but can be accessed by scrolling down. The newly added green control panels include Demultiplexing Controls, HT Parameters, FT Parameters, and Ion Mobility Parameters and are shown to the far right.

CODE AVAILABILITY

The UniChromCD module has been added to the open-source UniDec software package and is freely available on GitHub: https://github.com/michaelmarty/UniDec. It is distributed under a modified BSD 3-clause license that permits unlimited private or commercial use and modification. No limits are placed on numbers of downloads and installations, and redistribution, including commercial redistribution, is permitted with proper attribution (detailed in the license).

UniDec can be downloaded as a compiled stand-alone Windows graphical user interface (GUI) or as a Python distribution, which also supports Mac and Linux operating systems. When using the Python distribution, UniChromCD can be run through the Launcher.py GUI or by directly running the UniCromCD.py script. A video tutorial has been posted to demonstrate its use: https://youtu.be/exrAdR-0iHs.

METHODS

Instrumentation, Sample Preparation, and Data Collection

The instrumentation used to generate the example SEC-MS data presented in this manuscript is described in detail in a companion paper,[29] so only a brief description is provided here. β-galactosidase and GroEL were purchased from Sigma or expressed and purified as described previously.[30] Glutamate dehydrogenase was purchased from Sigma. All samples were buffer exchanged into 0.2 M ammonium acetate (Sigma) using Biospin P6 (BioRad) spin columns and diluted to 0.1 – 0.5 mg/mL. The sample concentration was optimized by diluting the sample to achieve the right level of ions in the CD-MS measurement. Measurements were collected in triplicate, and a single representative spectrum is usually shown. Only a single replicate of the Shift 15 data was collected because it did not yield usable data, as discussed below.

Online SEC used an Agilent 1100 quaternary pump connected to a 6-port switching valve, which was equipped with a 100 µL sample loop and controlled by an Arduino microcontroller. The column used was a Superose 6 Increase 5/150, which has a broad fractionation range ideal for the proteins used, and the flow of 200 mM ammonium acetate was maintained at 0.2 mL/min. Each injection was for 1.5 s, which yielded a 5 µL injection, and the total cycle time was 1 min. These parameters were optimized based on the resolution of the column to achieve good peak density, distinct peaks, and minimal total analysis time. CD-MS data were acquired in Direct Mass Technology (DMT) mode on a Q Exactive HF UHMR Orbitrap mass spectrometer (Thermo Scientific Instruments) using a resolution setting of 240,000 at *m/z* 400 (512 ms transient length) and fixed ion injection times between 50 and 200 ms, which were optimized to achieve a single ion level. Additional details can be found in the accompanying manuscript.[29]

The IM instrument was an atmospheric pressure dual-gate drift tube constructed from printed circuit boards, according to the design published by Clowers *et al.*[31] A drift voltage of 4 kV was applied, corresponding to an electric field strength of 200 V/cm. The ion gates were controlled by applying a voltage of 75 V (front) or 85 V (back) above the standard potential at their respective locations using a pair of FET pulsers built by GAA Custom Engineering (Kennewick, WA). Frequency sweeps, ranging from 5 Hz to 505 Hz, were generated by custom Python scripts. Gating waveforms were applied using an Arduino-compatible microcontroller (Wio Terminal, Seeedstudio) and synchronized with the MS scans using the split lens signal output as a trigger, as previously described.[32] Additionally, a voltage

level shifter was used to accommodate the different signal levels from the MS and the Arduino microcontroller. CD-MS data were acquired on a Q Exactive UHMR Orbitrap mass spectrometer using a resolution setting of 100,000 at *m/z* 400. Fixed ion injection times between 400 and 600 ms were used. Additional details can be found in an accompanying manuscript.[33]

Software Overview

UniChromCD was programmed as a new module within the UniDec software package. It is built entirely in Python, using libraries such as numpy,[34] scipy,[35] matplotlib,[36] and wxPython (version 4.2). It is designed with a model-presenter-view architecture, where the model is a backend application programming interface (API) that can be accessed through Python scripting (HTEng.py), the view is a wxPython frontend GUI, and the presenter (UniChromCD.py) controls the overall program flow by connecting the front and backends.

UCCD inherits many of the same functions and GUI elements as UniDecCD, the module for analysis of individual CD-MS spectra.[37] For example, the frontend GUI is the same as UniDecCD but includes added panels for demultiplexing and additional plotting panels, as shown in **Figure 1**. The presenter (UniChromCDApp) inherits the presenter from UniDecCD (UniDecCDApp) and includes additional functions to make use of the new frontend features. The backend engine

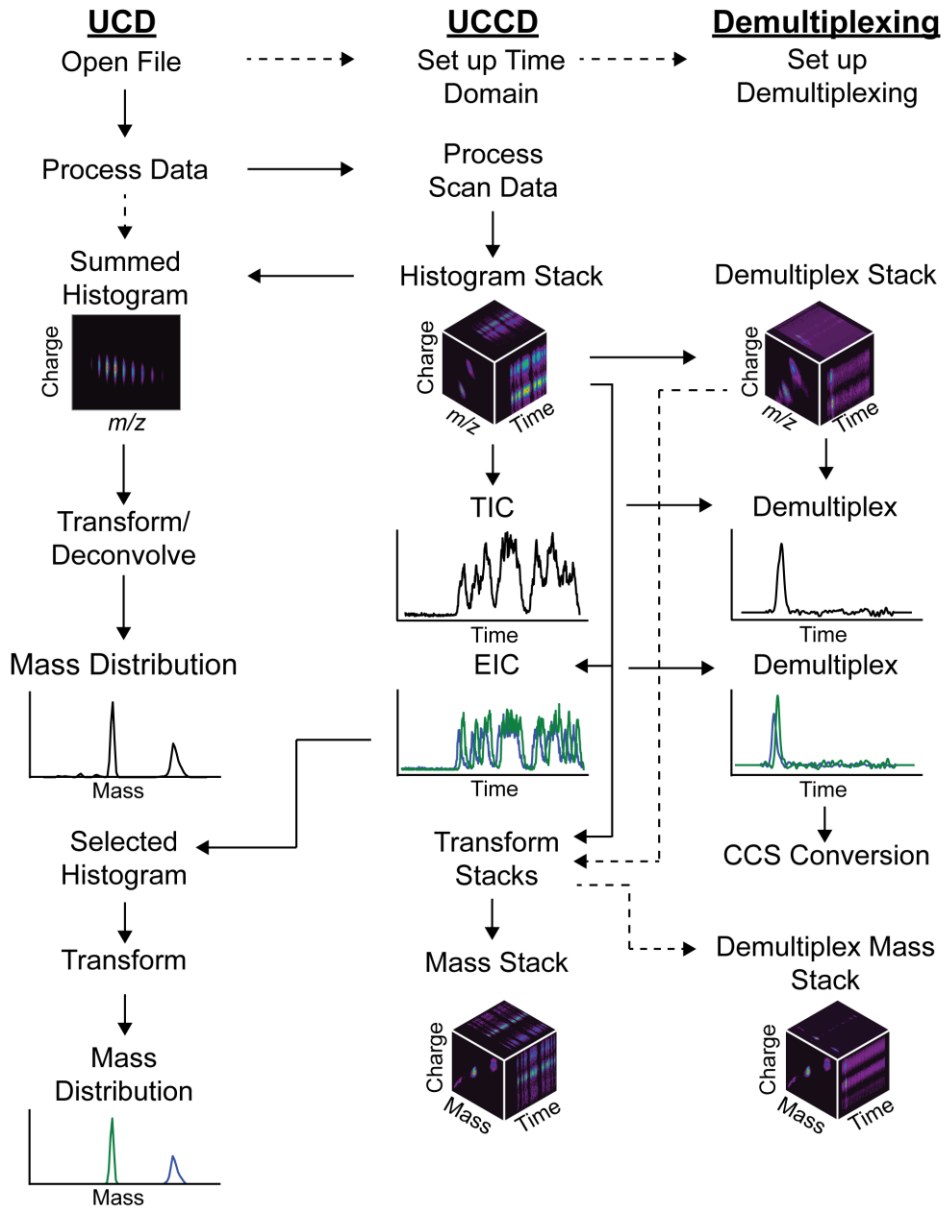

Figure 2. Flowchart showing the data flow and interactions between the different programming classes of UCCD. Files are opened using the existing UniDecCD (UCD) code, but new elements in UCCD and the demultiplexing engine (DM) set up the required time-domain information and prepare the demultiplexing kernels. After the data is processed in UCD, UCCD parses the processed data into a histogram stack and creates the TIC. EICs can be extracted from the summed histogram, which can then be processed with UCD to yield extracted mass distributions. The entire histogram stack can also be transformed to convert the m/z axis to mass. At any point, the TIC, EIC, m/z histogram stack, or mass histogram stack can be demultiplexed. EICs from FT-IM data can be further converted from drift time into CCS.

(UniChromCDEng) inherits the engine from UniDecCD (UniDecCD) and the additional demultiplexing class (HTEng). Thus, the UCCD engine contains three primary components, the prior UniDecCD functions, new time-domain UCCD functions, and new demultiplexing functions. The relationship between these different types of code is shown in **Figure 2** and described below.

From UniDecCD, UCCD inherits the existing tools for opening, processing, transforming, and deconvolving CD-MS data of various types (**Figure 2**, *left*). The new UCCD engine (**Figure 2**, *center*) class adds time-domain processing of CD-MS scans to generate histogram stacks, which are 3D data sets of *m/z* vs. charge vs. time. It includes new tools for creating total ion chromatograms (TICs) and extracted ion chromatograms (EICs) from the CD-MS data. It also includes new functions to transform the *m/z* axis on histogram stacks to a mass axis. Existing UniDecCD tools are repurposed to transform extracted histograms in isolation.

Finally, UCCD also inherits a new demultiplexing engine (**Figure 2**, *right*). The demultiplexing engine includes tools to set up both HT and FT demultiplexing. It operates on individual TICs or EICs. However, the UCCD engine can also pass each pixel from the histogram stack (either the *m/z* or mass histogram stack) to demultiplex the entire stack (see Supplementary Information). For FT-IM data, demultiplexed mobiligrams can be converted from drift time to collision cross section (CCS).

This overall architecture allowed us to reuse a lot of the same code from UniDecCD while providing a flexible platform to build new tools into it. For example, as new demultiplexing options were added, we simply added them to the demultiplexing class and did not have to make any edits to the UCCD class. Additional details on each of the key features of the workflow are described below and in the Supporting Information.

Data Import and Processing

UniDec can open a range of different file types, including Thermo Raw, DMT, mzML, and several text/binary formats. UCCD uses the same algorithm as UniDecCD for data processing and charge assignment, as previously described.[37] When the data is imported, a TIC is automatically created. EICs can be created by the user selecting a square or "swoop" region (**Figure 1**) of the *m/z* vs. charge histogram. Additional details can be found in the Supplementary Information. Although we focus here on the novel demultiplexing aspects of the software, UCCD provides a user-friendly interface for analysis and visualization of conventional time-resolved CD-MS.

HT Demultiplexing

The theory behind HT demultiplexing has been described in detail previously.[19,20,24,25,38,39] The core of the implementation used here is a convolution of the HT kernel (described in the Supplementary Information) with the multiplexed chromatogram, which uses the Fourier convolution theorem:

$$Y = \mathcal{F}^{-1}(\mathcal{F}(X) \times \mathcal{F}(K)^{*}) \qquad (1)$$

Where Y is the demultiplexed chromatogram, X is the multiplexed chromatogram, K is the HT kernel, $\mathcal{F}$ denotes a Fourier transform, $\mathcal{F}^{-1}$ denotes an inverse Fourier transform, and $\mathcal{F}(K)^{*}$ is the complex conjugate of $\mathcal{F}(K)$. Details on pseudo random binary sequences and construction of the HT kernel can be found in the Supplemental Information.

Because retention times in LC are typically much longer than the desired cycle time (the time interval between injections), it is usually necessary to extend the acquisition beyond the end of the injection sequence. For convenience, this is accomplished by appending zeros to the end of the sequence so that the end of the expanded sequence occurs after the last peak has fully eluted. It is important to note that these added zeros are *not* used in the construction of the HT kernel and therefore do not violate the requirement[40] that the number of zeros in the kernel PRBS be 2^{m-1}-1. Prior to demultiplexing, the appended zeros are moved from the end of the sequence to the beginning, which in turn shifts the original PRBS to the end of the chromatogram, where ideally it completely overlaps with the portion of the chromatogram that contains peaks. In cases where the difference in retention time between two or more peaks in the chromatogram are greater than the cycle time, it may be necessary to manually adjust this time shift during processing of chromatograms to ensure complete overlap of the HT kernel with the data. To help check alignment, the kernel can be plotted over the raw chromatograms using Tools > Plot Kernel.

FT Demultiplexing

The use of FT demultiplexing to couple IM with MS has been described extensively in the literature.[25,26,41–44] In brief, ions traversing the separation region of a spatially dispersive IM instrument are controlled by a pair of ion gates at the entrance and exit. The gates are modulated simultaneously according to a square wave that linearly or iteratively increases in frequency, typically from 5 Hz to several hundred or thousand Hz over the course of the experiment. As a result, the intensity of the chromatogram oscillates with a frequency related to its drift time by Equation 2:

$$t_d = \frac{sweep\ rate}{f} \qquad (2)$$

Where t_d is the ions drift time between gates in seconds, *sweep rate* is the rate at which the gating frequency was swept in Hz/second, and f is the frequency of the chromatogram oscillation. In UCCD, FT-IM data is treated like HT-SEC data before and after the demultiplexing stage. The program simply uses a different algorithm to demultiplex the data.

Prior to Fourier transformation, the oscillating ion signal can be processed in several ways that are described briefly here and in more detail in the Supplementary Information. Scan compression can be applied to allow for the collection of multiple CD-MS scans at each point of the gating frequency sweep. Chromatograms can be apodized using the second half of a Hanning function and zero padded to increase the sampling density of the FT. The chromatogram can be "flattened" to remove the large low-frequency component in the frequency domain often caused by signal decay in the time domain.

Following pre-processing, total or extracted ion chromatograms are Fourier transformed, and the resulting frequency axis is converted to drift time using Equation 2 to create arrival time distributions. The *sweep rate* parameter is calculated from the start and end frequencies and analysis time, which are entered by the user. In the current implementation, a simple implementation of absorption mode processing[44] is achieved by calculating the phase at the apex of each ATD and applied consistently throughout the drift time range. When multiple ATDs are demultiplexed, phases are calculated for each individually. Future versions will explore dynamic phase correction, as described

previously.[44] Finally, collision cross section (CCS) axes can be calculated for individual EICs, as described in the Supplementary Information.

RESULTS AND DISCUSSION

HT-SEC-CD-MS Workflow

To illustrate a typical HT-SEC-CD-MS workflow, we collected data for a simple mixture of β-galactosidase and GroEL. The sample was injected according to a 5-bit sequence as described in a companion paper.[29] Here, we focus on data with a 5-bit injection sequence because it produced excellent quality data in a relatively short time, but additional bit lengths are shown in that paper.[29] When raw CD-MS data is imported for the first time, the three plots shown in **Figure 3A, B,** and **C** are automatically generated. The raw chromatogram (**Figure 3A**) appears noisy because each individual scan contains only a few ions. This low number of ions causes inherent shot noise variability between scans. Similarly, the *m/z* (**Figure 3B**) and mass (**Figure 3C**) distributions are too finely sampled and do not contain enough ion counts per bin. Setting the Scan Compression to 10, *m/z* Bin Size to 10, and Mass Bin Size to 20 kDa produces smoother distributions, shown in **Figure 3D, E,** and **F**.

Note, the Scan Compression and Mass Bin Size parameters are independent of the others. In other words, adjusting the scan compression will only affect chromatography data (**Figure 3A**, **D**) and will not affect the total number of ions in the *m/z* vs. charge histograms (**Figure 3B**, **E**) or the transformed mass distributions (**Figure 3C**, **F**). Changing the *m/z* binning will affect the potential resolution of the mass bins, but neither binning

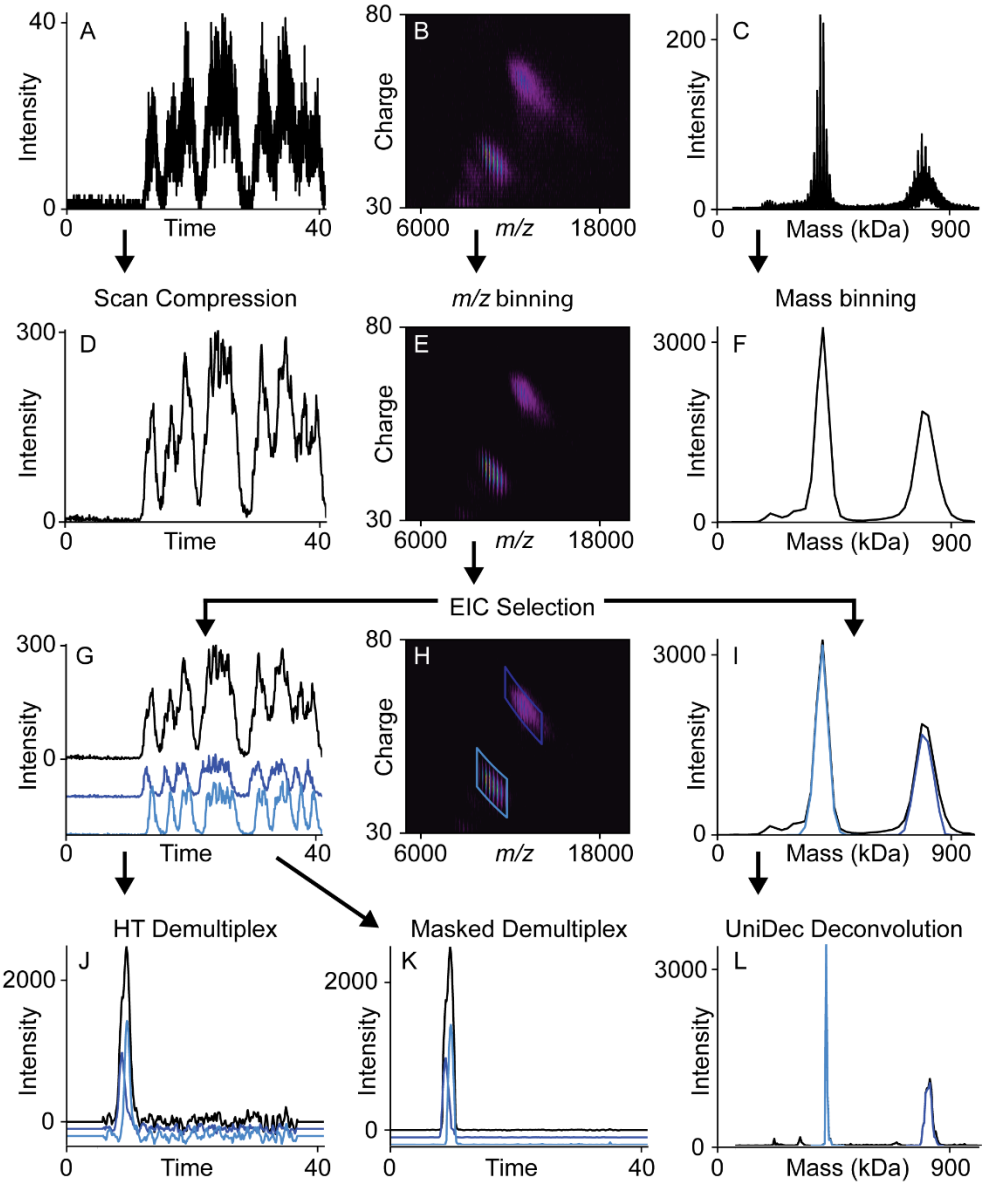

Figure 3. Schematic of a typical HT-SEC-CD-MS workflow. (A) Raw TIC, (B) 2D m/z vs. charge histogram, and (C) mass distribution plots are generated when the data is opened. Scan compression of (A) produces a smoother chromatogram (D). Binning the m/z values in (E) smooths the histogram (E). Binning the mass values in (C) smooths the mass distribution (F). Selecting a region of the histogram (H) generates EICs (G) and the extracted mass distributions (I) for each selected species. If the data is deconvolved by UCD, the extracted masses will also be deconvolved (L). TICs and EICs can be demultiplexed (J), which can then be further improved by masked demultiplexing (K).

parameter will affect the chromatography data because the total number of ions per scan is preserved.

Next, EICs are generated by either simple range selection (generating a square selection window in *m/z* and charge) or "swoop" selection (generating a diagonal selection window that follows the natural *m/z* trend lines), as shown in **Figure 3H**. After selecting the *m/z* distribution, UCCD produces the raw EICs (**Figure 3G**) and extracted mass distributions of the selected ranges (**Figure 3I**). Currently, we have not implemented per-scan UCD deconvolution[37] of each histogram in the stack. However, deconvolution of the summed histogram can be performed, and extracted mass distributions can be generated from this deconvolved summed distribution (**Figure 3L**).

After generating the TIC or EICs, HT demultiplexing can be applied to the chromatograms to produce demultiplexed chromatograms (**Figure 3J**). Although the two species are not resolved in the demultiplexed TIC, the demultiplexed EICs show separation with the expected elution order. The baseline illustrates the application of the Time Shift parameter discussed above. The baseline from the demultiplexed data is bracketed by flat sections that are automatically added to compensate for the zero pads used in the acquisition. Thus, the total chromatogram with included zero pads is the same length as the original data. However, there is an option in UCCD to define the time range to truncate the chromatograms to remove the unneeded baseline beyond when the peaks elute.

In practice, we found that TIC and EIC demultiplexing were mostly natural to use. However, there is an option to perform per-pixel demultiplexing. Here, an EIC is generated for each *m/z* vs. charge pixel in the histogram stack. Each pixel EIC is demultiplexed independently and then reassembled into a 3D demultiplexed histogram stack (**Figure 2**). The same process can also be performed on a transformed mass histogram stack, which has been converted first into mass vs. charge vs. time. Both operations allow users to produce an EIC by selecting a mass range. Interestingly, summing each time point of the per-pixel demultiplexing perfectly reproduces the demultiplexed TIC, revealing that the total number of ions in conserved in the demultiplexing operation.

HT Artifact Removal

In addition to the core demultiplexing features, we have included tools to remove HT demultiplexing artifacts. These artifacts are caused by noise and imperfections between the peaks, which should ideally be perfectly repeated copies of each other. For example, if one peak is randomly larger than the others, this will cause baseline artifacts during demultiplexing. Systematic drifts, such as a gradual decrease in signal, also cause similar artifacts.

To remove these baseline artifacts, we employed a masked multiplexing strategy developed by Clowers *et al.* for HT-IM data.[45] This option is easily activated by changing the Demultiplex Mode parameter from "HT" to "mHT". The masked multiplexing is defined by setting the number of iterations, which defines how many sets of random masks are created (**Figure S1**), and the number of masks per iteration, which defines how many digits are masked in each set of masks. We found that 50 iterations and 5 masks per iteration significantly cleaned up demultiplexing artifacts without distorting the primary peaks (**Figure 3K**, **Figure S1C**). Together, these tools provide a robust and user-friendly workflow for processing HT-SEC-CD-MS data.

HT-SEC-CD-MS Sequence Shifting

Many of the PRBSs from Harwit *et al*.[40] place the largest continuous string of zeros at the beginning of the sequence. The leading zeros have the unfortunate effect of delaying the first injection by several minutes, creating unnecessary dead time at the beginning of the chromatogram. Because the Hadamard transform demultiplexing operation is circular in nature, we hypothesized that it should be possible to rotate these sequences so that the longest stretch of zeros falls at the end of the sequence. Putting the zeros at the end reduces initial dead time and reduces the number of zero pads that must be used because the last injection occurs earlier in the sequence. Therefore, the total analysis time can be shortened significantly.

To evaluate this approach, we repeated the 5-bit injection of β-galactosidase and GroEL using two modified sequences: the first rotating the sequence four positions to the left to move the first four zeros to the end of the sequence (termed "shift 4") and the second rotating the original sequence 15 positions ("shift 15") to split the longest stretch of ones (see Supplemental Methods). The shift 4 chromatogram (**Figure S2C**) is like the original but with everything 4 minutes earlier, including the end of the acquisition. As expected, the shift 4 sequence produced a demultiplexed chromatogram (**Figure S2D**) that is nearly identical to the one produced with the original sequence (**Figure S2B**).

In contrast, the demultiplexed chromatogram from the shift 15 sequence (**Figure S2E**) contains significantly more artifacts than either the original or the shift 4 sequence. These artifacts are caused by an inability to fully overlap the HT kernel and raw chromatogram. In the data produced by the original and shift 4 sequences (**Figure S2A** and **C**), the kernel completely overlaps all the peaks in the chromatogram. However, the shift 15 sequence starts and ends with an injection, producing a chromatogram (**Figure S2E**) where the first and last peaks are separated by an additional four minutes compared to the other two sequences, which have four zeros at the beginning or end. Because the kernel does not fully overlap with all chromatographic peaks, not all peaks are included in the demultiplexing, which causes the artifacts in **Figure S2F**.

Although incomplete kernel overlap is easily avoided by rotating the sequence to place the largest block of zeros at the beginning or end, it illustrates a potential limitation of HT demultiplexing method that could arise if the separation of two analytes is greater than the maximum number of consecutive zeros in the sequence times the cycle time. In these cases, a longer sequence or cycle time would be required to ensure that the kernel can overlap the sequence completely.

FT-IM-CD-MS

The workflow for FT-IM-CD-MS is similar to the workflow for HT-SEC-CD-MS. The primary differences are the different parameters used for demultiplexing, the need for different types of chromatogram processing (e.g. apodization), and the potential to convert drift time to CCS after demultiplexing. To demonstrate the workflow, we collected FT-IM-CD-MS data of glutamate dehydrogenase (GDH), shown in **Figure 4**.

As with the HT-SEC data, the raw TIC (**Figure 4A**) is noisy due to high scan-to-scan variability. After conversion from frequency to drift time using **Equation 2**, the Fourier transform of the TIC (**Figure 4B**) shows a peak at the correct drift time, but it is somewhat sparsely sampled and contains a large low frequency component caused by the overall decay of the time

domain signal intensity (**Figure 4A**) that distorts the baseline of the arrival time distribution (ATD). Applying scan compression (**Figure 4C**) reduces noise and increases the total ion count per bin, as reflected by the increased intensity scale. Although scan compression improves the quality of the TIC, the Fourier transform of the compressed TIC is essentially unchanged (**Figure 4D**) because the information removed by scan compression is in the higher frequency region of the demultiplexed spectrum. Simply down-sampling the TIC without changing the total analysis time, sweep rate, or signal frequency, causes a truncation of the upper bound of the frequency spectrum (which is typically several octaves above the drift time peak) without changing the spacing of the FT bins.

To increase the sample density in the ATD, additional zeros can be added to the chromatogram. Along with zero padding, apodization was turned on, which is required when zero padding is used (see Supplemental Methods section for details). After zero padding and apodization, the chromatogram (**Figure 4E**) does not display the appended zeros but does clearly show the result of the "half window" apodization function that creates a smooth transition to zero intensity at the end of the chromatogram while preserving the large oscillations at the beginning. As shown in **Figure 4F,** the ATD is notably smoother due to the increased sampling density but shows a small increase in the baseline at lower frequencies.

To remove the low frequency artifact, the TIC can be "flattened" (**Figure 4G**) by first smoothing the chromatogram using an aggressive Savitzky-Golay filter and then subtracting the smoothed function from the original to center it around the x-axis. Flatting the chromatogram eliminates the low frequency artifact in the ATD (**Figure 4H**), bringing the baseline closer to zero. To further improve the data, absorption mode FT[44] can be used to produce a sharper peak with additional baseline reduction, as shown in **Figure 4J**.

Finally, as with HT-SEC, EICs can be selected from the 2D *m/z* vs charge histogram in the same manner described above (**Figure 4I**). If CCS calculations are desired, it is necessary to select single charge states because charge is a critical parameter in CCS calculation. Calculating CCS distributions from multiple charge states could yield incorrect CCS calculations, so swoop selections are not useful for this application. EICs are automatically plotted in both the raw and demultiplexed chromatogram window when selected (**Figure 4K**). Finally, the CCS distributions can be calculated from the drift time by using the experimental conditions input by the user (drift voltage, pressure, etc.). As shown in **Figure 4L**, the CCS distributions for each isolated charge state agree with expected CCS values and shift in the expected manner toward slightly higher CCS with higher charge states.[46] Together, these data demonstrate that UCCD provides a comprehensive and versatile workflow for FT-IM-CD-MS data analysis.

CONCLUSION

UniChromCD provides a comprehensive platform for analyzing time-resolved CD-MS data with or without multiplexing. The program is free and open source, allowing users control of their data and the ability to customize processing for new applications as they arise. We demonstrated the use of UCCD for demultiplexing and analysis of HT-SEC-CD-MS data of a mixture of proteins. The embedded masked multiplexing algorithm removes artifacts from HT demultiplexed chromatograms while preserving peak fidelity. Although we focused here on well-defined protein mixtures to illustrate how the software works, more complex samples of *E. coli.* lysate are shown in a companion manuscript,[29] demonstrating that the software performs well for complex and heterogeneous mixtures.

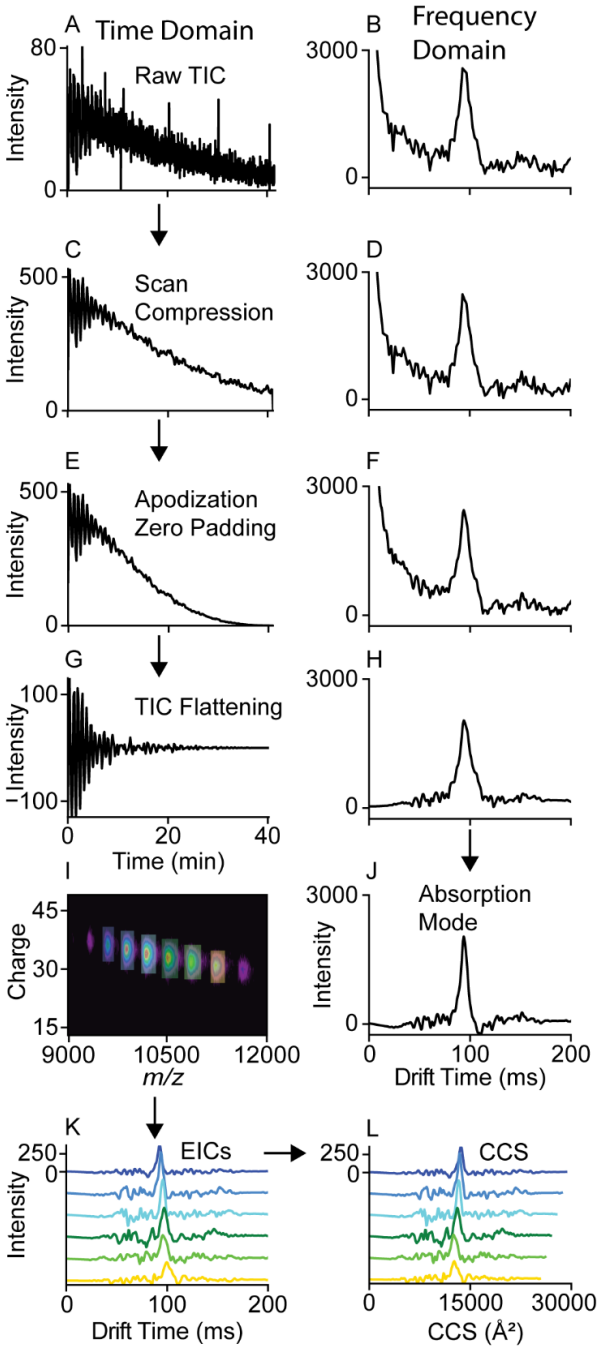

Figure 4. Typical FT-IM-CD-MS workflow. Raw TICs (A) are scan compressed (C) and then processed with apodization and zero padding (E). Flattening (G) the processed TIC removes the low frequency component. B, D, F, and H are the Fourier transforms of A, C, E, and G, respectively converted to drift time using **Eq. 2**. (I) 2D m/z vs. charge histogram with EIC selections shown with colored boxes. (J) Absorption mode processing of the ATD shown in H. (K) EIC ATDs from the selections in I. (L) ATDs from K converted to CCS.

We also showed demultiplexing of FT-IM-CD-MS data, which enables fast IM separations to be interfaced with slower

CD-MS acquisitions. Here, UCCD facilitates signal processing options such as zero padding, apodization, and absorption mode processing. It also performs collision cross section calculations on selected charge states. In both types of experiments, UCCD demultiplexing recovers retention/drift time information while significantly increasing CD-MS throughput. We anticipate that these new computational tools will enable a range of emerging applications coupling CD-MS with time-domain separations, especially to characterize complex biotherapeutics and heterogeneous protein complexes.

ASSOCIATED CONTENT

Supporting Information

The Supporting Information is available free of charge on the ACS Publications website.

Supplemental methods on data import and processing, HT processing, and FT processing; supplemental figures with raw and demultiplexed TICs of standard 5-bit, shift 4, and shift 15 PRBSs and chromatograms from the masked multiplex process.

AUTHOR INFORMATION

Corresponding Author

* mtmarty@arizona.edu

NOTES

All raw data for this manuscript is available at MassIVE, with HT-SEC data at MSV000095091 (DOI: 10.25345/C5FN1139K) and FT-IM data as MSV000095092 (DOI: 10.25345/C59W0996X). A video tutorial is available at: https://youtu.be/exrAdR-0iHs. Code is available for free download at: https://github.com/michaelmarty/UniDec.

ACKNOWLEDGMENT

The authors thank Maria Reinhardt-Szyba, Kyle Fort, Mike Senko, and Alexander Makarov at Thermo Fisher Scientific for their support on the Q-Exactive UHMR instruments and DMT mode acquisition. The authors thank Marielle Walti and Abigail Page for donating the GroEL plasmid and guidance in its expression and purification, and Jennifer Brodbelt for supplying the instruments used to collect ion mobility data. This work was funded by the National Science Foundation under grants CHE-1845230 and CHE-2403561 (MTM) and CHE-2203602 (Brodbelt).

REFERENCES

(1) Pierson, E. E.; Contino, N. C.; Keifer, D. Z.; Jarrold, M. F. Charge Detection Mass Spectrometry for Single Ions with an Uncertainty in the Charge Measurement of 0.65 e. *J. Am. Soc. Mass Spectrom.* **2015**, *26* (7), 1213–1220. https://doi.org/10.1007/s13361-015-1126-x.

(2) Deslignière, E.; Rolland, A.; Ebberink, E. H. T. M.; Yin, V.; Heck, A. J. R. Orbitrap-Based Mass and Charge Analysis of Single Molecules. *Acc. Chem. Res.* **2023**, *56* (12), 1458–1468. https://doi.org/10.1021/acs.accounts.3c00079.

(3) Kafader, J. O.; Melani, R. D.; Senko, M. W.; Makarov, A. A.; Kelleher, N. L.; Compton, P. D. Measurement of Individual Ions Sharply Increases the Resolution of Orbitrap Mass Spectra of Proteins. *Anal. Chem.* **2019**. https://doi.org/10.1021/acs.analchem.8b04519.

(4) Harper, C. C.; Elliott, A. G.; Oltrogge, L. M.; Savage, D. F.; Williams, E. R. Multiplexed Charge Detection Mass Spectrometry for High-Throughput Single Ion Analysis of Large Molecules. *Anal. Chem.* **2019**, *91* (11), 7458–7465. https://doi.org/10.1021/acs.analchem.9b01669.

(5) Miller, L. M.; Jarrold, M. F. Charge Detection Mass Spectrometry for the Analysis of Viruses and Virus-like Particles. *Essays Biochem.* **2023**, *67* (2), 315–323. https://doi.org/10.1042/EBC20220101.

(6) Kostelic, M. M.; Ryan, J. P.; Brown, L. S.; Jackson, T. W.; Hsieh, C.-C.; Zak, C. K.; Sanders, H. M.; Liu, Y.; Chen, V. S.; Byrne, M.; Aspinwall, C. A.; Baker, E. S.; Marty, M. T. Stability and Dissociation of Adeno-Associated Viral Capsids by Variable Temperature-Charge Detection-Mass Spectrometry. *Anal. Chem.* **2022**, *94* (34), 11723–11727. https://doi.org/10.1021/acs.analchem.2c02378.

(7) Lutomski, C. A.; Gordon, S. M.; Remaley, A. T.; Jarrold, M. F. Resolution of Lipoprotein Subclasses by Charge Detection Mass Spectrometry. *Anal. Chem.* **2018**, *90* (11), 6353–6356. https://doi.org/10.1021/acs.analchem.8b01127.

(8) Brown, B. A.; Zeng, X.; Todd, A. R.; Barnes, L. F.; Winstone, J. M. A.; Trinidad, J. C.; Novotny, M. V.; Jarrold, M. F.; Clemmer, D. E. Charge Detection Mass Spectrometry Measurements of Exosomes and Other Extracellular Particles Enriched from Bovine Milk. *Anal. Chem.* **2020**, *92* (4), 3285–3292. https://doi.org/10.1021/acs.analchem.9b05173.

(9) Harper, C. C.; Miller, Z. M.; McPartlan, M. S.; Jordan, J. S.; Pedder, R. E.; Williams, E. R. Accurate Sizing of Nanoparticles Using a High-Throughput Charge Detection Mass Spectrometer without Energy Selection. *ACS Nano* **2023**, *17* (8), 7765–7774. https://doi.org/10.1021/acsnano.3c00539.

(10) den Boer, M. A.; Lai, S.-H.; Xue, X.; van Kampen, M. D.; Bleijlevens, B.; Heck, A. J. R. Comparative Analysis of Antibodies and Heavily Glycosylated Macromolecular Immune Complexes by Size-Exclusion Chromatography Multi-Angle Light Scattering, Native Charge Detection Mass Spectrometry, and Mass Photometry. *Anal. Chem.* **2022**, *94* (2), 892–900. https://doi.org/10.1021/acs.analchem.1c03656.

(11) Strasser, L.; Füssl, F.; Morgan, T. E.; Carillo, S.; Bones, J. Exploring Charge-Detection Mass Spectrometry on Chromatographic Time Scales. *Anal. Chem.* **2023**. https://doi.org/10.1021/acs.analchem.3c03325.

(12) Yin, V.; Deslignière, E.; Mokiem, N.; Gazi, I.; Lood, R.; de Haas, C. J. C.; Rooijakkers, S. H. M.; Heck, A. J. R. Not All Arms of IgM Are Equal: Following Hinge-Directed Cleavage by Online Native SEC-Orbitrap-Based CDMS. *J. Am. Soc. Mass Spectrom.* **2024**. https://doi.org/10.1021/jasms.4c00094.

(13) McGee, J. P.; Senko, M. W.; Jooß, K.; Des Soye, B. J.; Compton, P. D.; Kelleher, N. L.; Kafader, J. O. Automated Control of Injection Times for Unattended Acquisition of Multiplexed Individual Ion Mass Spectra. *Anal. Chem.* **2022**, *94* (48), 16543–16548. https://doi.org/10.1021/acs.analchem.2c03495.

(14) Elliott, A. G.; Harper, C. C.; Lin, H.-W.; Susa, A. C.; Xia, Z.; Williams, E. R. Simultaneous Measurements of Mass and Collisional Cross-Section of Single Ions with Charge Detection Mass Spectrometry. *Anal. Chem.* **2017**, *89* (14), 7701–7708. https://doi.org/10.1021/acs.analchem.7b01675.

(15) G. Elliott, A.; C. Harper, C.; Lin, H.-W.; R. Williams, E. Mass, Mobility and MS n Measurements of Single Ions Using Charge Detection Mass Spectrometry. *Analyst* **2017**, *142* (15), 2760–2769. https://doi.org/10.1039/C7AN00618G.

(16) Fisher, N. P.; McGee, J. P.; Bowen, K. P.; Goodwin, M.; Senko, M. W.; Kelleher, N. L.; Kafader, J. O. Determining Collisional Cross Sections from Ion Decay with Individual Ion Mass Spectrometry. *J. Am. Soc. Mass Spectrom.* **2023**, *34* (12), 2625–2629. https://doi.org/10.1021/jasms.3c00340.

(17) Fan, Z.; Lin, C.-H.; Chang, H.-W.; Kaneta, T.; Lin, C.-H. Design and Application of Hadamard-Injectors Coupled with Gas and Supercritical Fluid Sample Collection Systems in Hadamard Transform-Gas Chromatography/Mass Spectrometry. *J. Chromatogr. A* **2010**, *1217* (5), 755–760. https://doi.org/10.1016/j.chroma.2009.12.007.

(18) Fan, G.-T.; Yang, C.-L.; Lin, C.-H.; Chen, C.-C.; Shih, C.-H. Applications of Hadamard Transform-Gas Chromatography/Mass Spectrometry to the Detection of Acetone in Healthy Human and Diabetes Mellitus Patient Breath. *Talanta*

2014, *120*, 386–390. https://doi.org/10.1016/j.talanta.2013.12.025.

(19) Lin, C.-H.; Kaneta, T.; Chen, H.-M.; Chen, W.-X.; Chang, H.-W.; Liu, J.-T. Applications of Hadamard Transform to Gas Chromatography/Mass Spectrometry and Liquid Chromatography/Mass Spectrometry. *Anal. Chem.* **2008**, *80* (15), 5755–5759. https://doi.org/10.1021/ac800201r.

(20) Siegle, A. F.; Trapp, O. Development of a Straightforward and Robust Technique to Implement Hadamard Encoded Multiplexing to High-Performance Liquid Chromatography. *Anal. Chem.* **2014**, *86* (21), 10828–10833. https://doi.org/10.1021/ac502933f.

(21) Kaneta, T.; Yamaguchi, Y.; Imasaka, T. Hadamard Transform Capillary Electrophoresis. *Anal. Chem.* **1999**, *71* (23), 5444–5446. https://doi.org/10.1021/ac990625j.

(22) Kaneta, T.; Kosai, K.; Imasaka, T. Ultratrace Analysis Based on Hadamard Transform Capillary Electrophoresis. *Anal. Chem.* **2002**, *74* (10), 2257–2260. https://doi.org/10.1021/ac011149b.

(23) Ibrahim, Y. M.; Garimella, S. V. B.; Prost, S. A.; Wojcik, R.; Norheim, R. V.; Baker, E. S.; Rusyn, I.; Smith, R. D. Development of an Ion Mobility Spectrometry-Orbitrap Mass Spectrometer Platform. *Anal. Chem.* **2016**, *88* (24), 12152–12160. https://doi.org/10.1021/acs.analchem.6b03027.

(24) Clowers, B. H.; Siems, W. F.; Hill, H. H.; Massick, S. M. Hadamard Transform Ion Mobility Spectrometry. *Anal. Chem.* **2006**, *78* (1), 44–51. https://doi.org/10.1021/ac050615k.

(25) Reinecke, T.; Naylor, C. N.; Clowers, B. H. Ion Multiplexing: Maximizing Throughput and Signal to Noise Ratio for Ion Mobility Spectrometry. *TrAC Trends Anal. Chem.* **2019**, *116*, 340–345. https://doi.org/10.1016/j.trac.2019.03.014.

(26) Poltash, M. L.; McCabe, J. W.; Shirzadeh, M.; Laganowsky, A.; Clowers, B. H.; Russell, D. H. Fourier Transform-Ion Mobility-Orbitrap Mass Spectrometer: A Next-Generation Instrument for Native Mass Spectrometry. *Anal. Chem.* **2018**, *90* (17), 10472–10478. https://doi.org/10.1021/acs.analchem.8b02463.

(27) Keelor, J. D.; Zambrzycki, S.; Li, A.; Clowers, B. H.; Fernández, F. M. Atmospheric Pressure Drift Tube Ion Mobility–Orbitrap Mass Spectrometry: Initial Performance Characterization. *Anal. Chem.* **2017**, *89* (21), 11301–11309. https://doi.org/10.1021/acs.analchem.7b01866.

(28) Sanders, J. D.; Shields, S. W.; Escobar, E. E.; Lanzillotti, M. B.; Butalewicz, J. P.; James, V. K.; Blevins, M. S.; Sipe, S. N.; Brodbelt, J. S. Enhanced Ion Mobility Separation and Characterization of Isomeric Phosphatidylcholines Using Absorption Mode Fourier Transform Multiplexing and Ultraviolet Photodissociation Mass Spectrometry. *Anal. Chem.* **2022**, *94* (10), 4252–4259. https://doi.org/10.1021/acs.analchem.1c04711.

(29) Sanders, J.; Owen, O.; Tran, B.; Mosqueira, J.; Marty, M. Coupling Online Size Exclusion Chromatography with Charge Detection-Mass Spectrometry Using Hadamard Transform Multiplexing. ChemRxiv May 31, 2024. https://doi.org/10.26434/chemrxiv-2024-h08x5.

(30) Grason, J. P.; Gresham, J. S.; Lorimer, G. H. Setting the Chaperonin Timer: A Two-Stroke, Two-Speed, Protein Machine. *Proc. Natl. Acad. Sci. U. S. A.* **2008**, *105* (45), 17339–17344. https://doi.org/10.1073/pnas.0807418105.

(31) Reinecke, T.; Clowers, B. H. Implementation of a Flexible, Open-Source Platform for Ion Mobility Spectrometry. *HardwareX* **2018**, *4*, e00030. https://doi.org/10.1016/j.ohx.2018.e00030.

(32) Cabrera, E. R.; Clowers, B. H. Synchronized Stepped Frequency Modulation for Multiplexed Ion Mobility Measurements. *J. Am. Soc. Mass Spectrom.* **2022**, *33* (3), 557–564. https://doi.org/10.1021/jasms.1c00365.

(33) Juetten, K.; Sanders, J.; Marty, M.; Brodbelt, J. Combining Fourier Transform Ion Mobility with Charge Detection Mass Spectrometry for the Analysis of Multimeric Protein Complexes. ChemRxiv July 1, 2024. https://doi.org/10.26434/chemrxiv-2024-cbqj1.

(34) Harris, C. R.; Millman, K. J.; van der Walt, S. J.; Gommers, R.; Virtanen, P.; Cournapeau, D.; Wieser, E.; Taylor, J.; Berg, S.; Smith, N. J.; Kern, R.; Picus, M.; Hoyer, S.; van Kerkwijk, M. H.; Brett, M.; Haldane, A.; del Río, J. F.; Wiebe, M.; Peterson, P.; Gérard-Marchant, P.; Sheppard, K.; Reddy, T.; Weckesser, W.; Abbasi, H.; Gohlke, C.; Oliphant, T. E. Array Programming with NumPy. *Nature* **2020**, *585* (7825), 357–362. https://doi.org/10.1038/s41586-020-2649-2.

(35) Virtanen, P.; Gommers, R.; Oliphant, T. E.; Haberland, M.; Reddy, T.; Cournapeau, D.; Burovski, E.; Peterson, P.; Weckesser, W.; Bright, J.; van der Walt, S. J.; Brett, M.; Wilson, J.; Millman, K. J.; Mayorov, N.; Nelson, A. R. J.; Jones, E.; Kern, R.; Larson, E.; Carey, C. J.; Polat, İ.; Feng, Y.; Moore, E. W.; VanderPlas, J.; Laxalde, D.; Perktold, J.; Cimrman, R.; Henriksen, I.; Quintero, E. A.; Harris, C. R.; Archibald, A. M.; Ribeiro, A. H.; Pedregosa, F.; van Mulbregt, P. SciPy 1.0: Fundamental Algorithms for Scientific Computing in Python. *Nat. Methods* **2020**, *17* (3), 261–272. https://doi.org/10.1038/s41592-019-0686-2.

(36) Hunter, J. D. Matplotlib: A 2D Graphics Environment. *Comput. Sci. Eng.* **2007**, *9* (3), 90–95. https://doi.org/10.1109/MCSE.2007.55.

(37) Kostelic, M. M.; Zak, C. K.; Liu, Y.; Chen, V. S.; Wu, Z.; Sivinski, J.; Chapman, E.; Marty, M. T. UniDecCD: Deconvolution of Charge Detection-Mass Spectrometry Data. *Anal. Chem.* **2021**, *93* (44), 14722–14729. https://doi.org/10.1021/acs.analchem.1c03181.

(38) Naylor, C. N.; Clowers, B. H.; Schlottmann, F.; Solle, N.; Zimmermann, S. Implementation of an Open-Source Multiplexing Ion Gate Control for High Kinetic Energy Ion Mobility Spectrometry (HiKE-IMS). *J. Am. Soc. Mass Spectrom.* **2023**, *34* (7), 1283–1294. https://doi.org/10.1021/jasms.3c00013.

(39) Pallmann, S.; Siegle, A. F.; Šteflová, J.; Trapp, O. Direct Hadamard Transform Capillary Zone Electrophoresis without Instrumental Modifications. *Anal. Chem.* **2018**, *90* (14), 8445–8453. https://doi.org/10.1021/acs.analchem.8b01010.

(40) Harwit, M.; Sloane, N. J. A. Chapter 3 - The Basic Theory of Hadamard Transform Spectrometers and Imagers. In *Hadamard Transform Optics*; Harwit, M., Sloane, N. J. A., Eds.; Academic Press, 1979; pp 44–95. https://doi.org/10.1016/B978-0-12-330050-8.50007-X.

(41) Knorr, F. J.; Eatherton, R. L.; Siems, W. F.; Hill, H. H. Fourier Transform Ion Mobility Spectrometry. *Anal. Chem.* **1985**, *57* (2), 402–406. https://doi.org/10.1021/ac50001a018.

(42) Keelor, J. D.; Zambrzycki, S.; Li, A.; Clowers, B. H.; Fernández, F. M. Atmospheric Pressure Drift Tube Ion Mobility–Orbitrap Mass Spectrometry: Initial Performance Characterization. *Anal. Chem.* **2017**, *89* (21), 11301–11309. https://doi.org/10.1021/acs.analchem.7b01866.

(43) Morrison, K. A.; Siems, W. F.; Clowers, B. H. Augmenting Ion Trap Mass Spectrometers Using a Frequency Modulated Drift Tube Ion Mobility Spectrometer. *Anal. Chem.* **2016**, *88* (6), 3121–3129. https://doi.org/10.1021/acs.analchem.5b04223.

(44) Sanders, J. D.; Butalewicz, J. P.; Clowers, B. H.; Brodbelt, J. S. Absorption Mode Fourier Transform Ion Mobility Mass Spectrometry Multiplexing Combined with Half-Window Apodization Windows Improves Resolution and Shortens Acquisition Times. *Anal. Chem.* **2021**, *93* (27), 9513–9520. https://doi.org/10.1021/acs.analchem.1c01427.

(45) Clowers, B. H.; Cabrera, E.; Anderson, G.; Deng, L.; Moser, K.; Van Aken, G.; DeBord, J. D. Masked Multiplexed Separations to Enhance Duty Cycle for Structures for Lossless Ion Manipulations. *Anal. Chem.* **2021**, *93* (14), 5727–5734. https://doi.org/10.1021/acs.analchem.0c04799.

(46) Bush, M. F.; Hall, Z.; Giles, K.; Hoyes, J.; Robinson, C. V.; Ruotolo, B. T. Collision Cross Sections of Proteins and Their Complexes: A Calibration Framework and Database for Gas-Phase Structural Biology. *Anal. Chem.* **2010**, *82* (22), 9557–9565. https://doi.org/10.1021/ac1022953.